

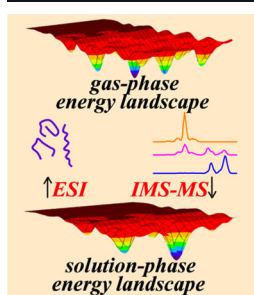
Ion Mobility-Mass Spectrometry Reveals the Energetics of Intermediates that Guide Polyproline Folding

Liuqing Shi,¹ Alison E. Holliday,² Matthew S. Glover,¹ Michael A. Ewing,¹ David H. Russell,³ David E. Clemmer¹

¹Department of Chemistry, Indiana University, Bloomington, IN 47405, USA

²Department of Chemistry, Moravian College, Bethlehem, PA 18018, USA

³Department of Chemistry, Texas A&M University, College Station, TX 77843, USA



Abstract. Proline favors *trans*-configured peptide bonds in native proteins. Although *cis/trans* configurations vary for non-native and unstructured states, solvent also influences these preferences. Water induces the all-*cis* right-handed polyproline-I (PPI) helix of polyproline to fold into the all-*trans* left-handed polyproline-II (PPII) helix. Our recent work has shown that this occurs via a sequential mechanism involving six resolved intermediates [Shi, L., Holliday, A.E., Shi, H., Zhu, F., Ewing, M.A., Russell, D.H., Clemmer, D.E.: Characterizing intermediates along the transition from PPI to PPII using ion mobility-mass spectrometry. *J. Am. Chem. Soc.* **136**, 12702–12711 (2014)]. Here, we use ion mobility-mass spectrometry to make the first detailed thermodynamic measurements of the folding intermediates, which inform us about

how and why this transition occurs. It appears that early intermediates are energetically favorable because of the hydration of the peptide backbone, whereas late intermediates are enthalpically unfavorable. However, folding continues, as the entropy of the system increases upon successive formation of each new structure. When PPII is immersed in 1-propanol, the PPII→PPI transition occurs, but this reaction occurs through a very different mechanism. Early on, the PPII population splits onto multiple pathways that eventually converge through a late intermediate that continues on to the folded PPI helix. Nearly every step is endothermic. Folding results from a stepwise increase in the disorder of the system, allowing a wide-scale search for a critical late intermediate. Overall, the data presented here allow us to establish the first experimentally determined energy surface for biopolymer folding as a function of solution environment.

Keywords: Energy landscape, Kinetics and thermodynamics, Biopolymer folding, Proline *cis/trans* isomerization

Received: 7 August 2015/Revised: 12 August 2015/Accepted: 14 August 2015

Introduction

Since Anfinsen's denaturation-renaturation experiments [1], biopolymer folding has been conceived as a cooperative two-state process, where the system spontaneously transforms from poorly-defined, less-structured, "denatured" configurations to the biologically-active "native" state, having a well-defined geometric structure [2]. This may occur along a single, energetically favorable pathway [3, 4], or it could involve many different paths that funnel the population toward an energy

minimum [2, 5, 6]. In more than 50 years of study, there is still a nearly complete dearth of experimental information about intermediates [2]—which must exist because folding occurs rapidly [2, 7]. Calculations provide insight about transitions; however, theory can only be directly tested against a limited set of experimental benchmarks [8, 9].

Ion mobility-mass spectrometry (IM-MS) is increasingly used to probe the structure and dynamics of biomolecules [10–13] and is especially sensitive to the *cis/trans* isomerization of proline residues [14–18]. In combination with theoretical approaches, conformations present in an ion mobility distribution can be identified, as measured collision cross sections can be compared with calculated values for theoretical geometries [19]. Furthermore, although it was first used for the study of gas-phase molecules, there is evidence that IM-MS can also provide insight about solution-phase structural

Electronic supplementary material The online version of this article (doi:10.1007/s13361-015-1255-2) contains supplementary material, which is available to authorized users.

Correspondence to: David Clemmer; e-mail: clemmer@indiana.edu

Published online: 11 September 2015

dynamics and heterogeneity [20–24]. Different solution conformations produce dissimilar gas-phase conformations upon desolvation from a gentle ionization source such as electrospray [25]; this enables detailed structural information about low-abundance and short-lived intermediates in solution to be accessed by IM-MS analysis.

Recently, we resolved and characterized numerous intermediates involved in folding the 13-residue polyproline (Pro13) from the all-*cis* polyproline-I (PPI) configuration to the all-*trans* polyproline-II (PPII) configuration [14]. The orientation of the peptide bond in polyproline is extremely sensitive to its environment [26–28]. In nonpolar solvents such as propanol, the peptide oligomer adopts the right-handed helical PPI structure in which every peptide bond orients adjacent pyrrolidine rings into a *cis* configuration [27, 29, 30], as is shown in Figure 1. This tightly-folded helix shields the peptide backbone from the solvent. Upon immersion in water, each bond flips into a *trans* orientation, resulting in the more extended, left-handed PPII helix. The hydrated structure is stabilized through interactions of exposed carbonyl groups along the peptide backbone with the polar solvent—a configuration that is also adopted by denatured and intrinsically disordered amino acid sequences [31–35].

Here, we extend our investigation to the PPII→PPI transition, showing that the reverse process is remarkably slow and proceeds via a different mechanism. The hypothetical energy landscape shown in Figure 1 illustrates the complex maze of pathways that arise upon *cis*→*trans* (PPI→PPII) or *trans*→*cis* (PPII→PPI) rotations of individual peptide bonds encountered in folding from one helix into the other. A stepwise mechanism would begin with rotation of a single peptide bond, leading to 12 possible *cis*–*trans* configurations. As folding proceeds, the number of possible configurational intermediates increases through a maximum of 924—all having six *cis* and six *trans*

peptide bonds, and then collapses again through fewer isomers to the new PPII helix. At minimum there are 479,001,600 (i.e., 12!) direct pathways between the PPI and PPII helices.

The preferred mechanism is determined by the energetics of intermediates and the barriers between them. Here, we present the first detailed thermodynamic measurements for peptide folding through observed intermediates. Kinetics and thermodynamic studies of helix formation provide a step-by-step understanding of the exquisite interplay between enthalpic and entropic forces and the role of solvent in guiding these transformations.

Experimental

Pro13 Peptide Synthesis

The Pro13 peptide was synthesized on a modified Applied Biosystems 430A synthesizer (Applied Biosystems, Foster City, CA, USA) by following a standard Boc solid-phase peptide synthesis protocol [36], as described previously [14].

Instrumentation

Ion mobility (IM) theory [19, 37–40] and instrumentation [11, 41–43] have been described elsewhere, and only a brief description is provided here. The instrument is comprised of a standard electrospray source, a ~1.8-m drift tube, and an orthogonal time-of-flight mass analyzer. A TriVersa NanoMate autosampler (Advion, Ithaca, NY, USA) was used to electrospray the sample into the ionization source, where ions were accumulated in an hourglass-shaped ion funnel [44] and periodically injected into the drift tube with a 150 μs wide pulse. The drift tube was filled with ~3 Torr of He buffer gas and maintained at a uniform electric field of ~10 V·cm⁻¹. Ions

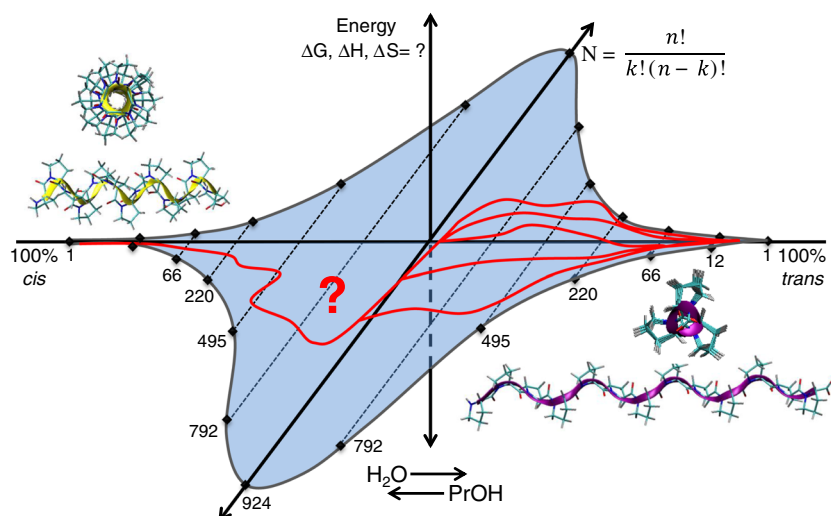


Figure 1. Hypothetical energy surface showing the number of possible *cis*–*trans* isomers (N) for Pro13. At each extreme, a single structural type is favored—the all-*cis* PPI form in propanol (left), or the all-*trans* PPII form in water (right). As the transition proceeds, the number of possible isomers increases and then decreases as folding continues. Experimental measurements of ΔG , ΔH , and ΔS provide insight about the details of why folding from one state to another occurs. The red lines show hypothetical pathways through preferred intermediates

were separated according to differences in their overall sizes and charge states while traveling down the drift tube. Upon exiting the drift tube, ions were extracted into the time-of-flight mass analyzer and subsequently detected. The data were collected in a nested fashion, as described previously [45].

Freeze Drying Conformations from Solution by Electrospray Ionization

A number of recent studies show that electrospray ionization (ESI) can produce species that retain elements of structures that are present in solution [14, 20, 21, 46–48]. Key to the present studies is that populations of *cis*–*trans* peptide configurations can be resolved as gaseous ions. The present study utilizes a home-built ESI source. Ions are dried as they transit a moderate pressure difference at room temperature. External electric fields are maintained such that heating of ions is minimized. The source capillary is not heated. Under these conditions, it is possible to retain information about populations of solution structures in these ESI ion populations that are produced. For additional insight, see Figure 2.

Determining Experimental Collision Cross Sections

The experimental collision cross sections can be obtained using Equation 1 [37],

$$\Omega = \frac{(18\pi)^{1/2}}{16} \frac{ze}{(k_b T)^{1/2}} \left[\frac{1}{m_I} + \frac{1}{m_B} \right]^{1/2} \frac{t_D E}{L} \frac{760}{P} \frac{T}{273.2} \frac{1}{N} \quad (1)$$

where ze is the ion's charge, k_b is Boltzmann's constant, and T is the temperature of the buffer gas; m_I and m_B refer to the masses of the ion and the buffer gas, respectively, and t_D is the experimental drift time of the ion. E , L , P , and N correspond to the applied electric field, the length of the drift region, the buffer gas pressure, and the neutral number density of the buffer gas at STP, respectively.

Kinetics Experiment

For the PPI→PPII transition, Pro13 peptides were initially dissolved in pure 1-propanol at a concentration of 160 μ M and incubated at 37°C for at least 72 h to ensure that all peptides were in the PPI configuration. The PPI→PPII transition was initiated by diluting the solution with water and acetic

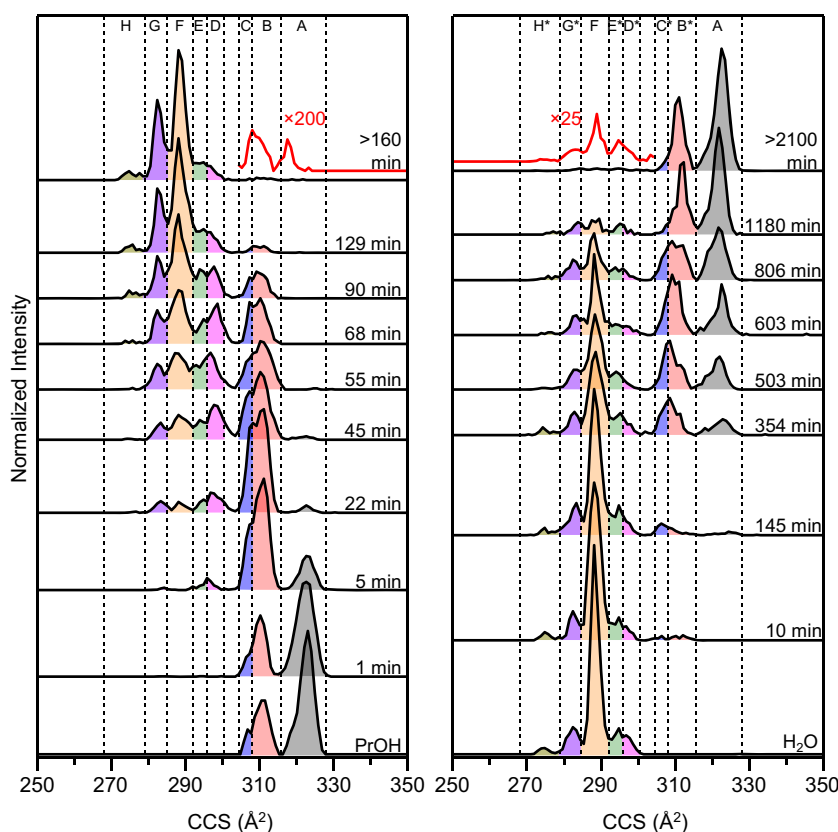


Figure 2. Cross section distributions for $[\text{Pro13} + 2\text{H}]^{2+}$ with time, showing the transition from PPI→PPII in 10:88:2 1-propanol:H₂O:HOAc (v:v:v) (left) and PPII→PPI in 97:1:2 1-propanol:H₂O:HOAc (v:v:v) (right) at 23°C. The regions of conformers are shown as different colors: A(black), B(red), C(blue), D(magenta), E(green), F(orange), G(violet), and H(olive). Initial distributions, obtained by electrospraying 98:2 1-propanol:HOAc and H₂O, respectively, are shown at the bottom of each panel. The inset (red) shows a blow up of low-abundance species present at equilibrium. Dashed lines delineate the cross section region for each conformer. The asterisk * indicates that the PPII→PPI conformer has the same cross section as found in the PPI→PPII direction, but may not have an identical structure. See text for details

acid (HOAc) to reach a solution composition of 10:88:2 (v:v:v) 1-propanol:H₂O:HOAc with a final Pro13 concentration of 16 μ M. A solution of 16 μ M Pro13 in 98:2 (v:v) 1-propanol:HOAc was also prepared for determining the initial solution population [14]. Acid was required here in order to maintain stable electrospray.

For the PPII \rightarrow PPI transition, Pro13 peptides were initially dissolved in pure water at 160 μ M concentration and incubated at 37°C for at least 72 h to ensure that all peptides were in the PPII configuration. The PPII \rightarrow PPI transition was initiated by diluting the solution with 1-propanol and HOAc to reach a solution composition of 97:2:1 (v:v:v) 1-propanol:HOAc:H₂O with a final Pro13 concentration at 16 μ M. A solution of 16 μ M Pro13 in H₂O was also prepared to determine the initial solution population for the reverse transition.

For both directions, the kinetics measurements were performed at five different temperatures (5, 15, 23, 35, and 45°C). Accordingly, the solution was incubated in a water bath at an appropriate temperature prior to and after the initiation of the transition until the end of the experiment. Aliquots of the solution were taken out at various transition times and placed into a sample tray maintained at 4°C for immediate analysis. The transition was done in quadruplicate at each temperature.

Kinetic Fitting of Conformer Abundance Profiles

The abundance of each conformer at each time point was characterized using OriginPro 9.0.0 software (OriginLab Corporation, Northampton, MA, USA). Individual peak areas were obtained using the Peak Analyzer function, and the relative abundance of each conformer was determined by dividing by the total peak area at that time point. Kinetic fitting of the relative abundance curves was accomplished using the Nonlinear Curve Fit tool by employing user-defined functions on the basis of first-order reaction rate laws. These mathematical functions were created to describe a series of possible routes for the transition and were generated using Maple 17.01 software (Waterloo Maple Inc., Waterloo, Canada). The abundances of the conformers in 98:2 (v:v) 1-propanol:HOAc (PPI \rightarrow PPII transition) or H₂O (PPII \rightarrow PPI transition) i.e., before initiation of the transition, were used as the initial and boundary condition during the fitting. For each fitting, the maximum number of iterations was 5×10^6 , and the tolerance was 1×10^{-15} .

Determination of Arrhenius Activation Parameters

The dependence of the rate constant (k) on the absolute temperature (T) is given by the Arrhenius equation (Equation 2),

$$\ln(k) = \frac{-E_a}{R} \frac{1}{T} + \ln(A) \quad (2)$$

where E_a is the activation barrier, A is the pre-exponential factor, and R is the universal gas constant. Using transition state theory, the enthalpy of activation (ΔH^\ddagger , Equation 3), the entropy of activation (ΔS^\ddagger , Equation 4), and the Gibbs free

energy of activation (ΔG^\ddagger , Equation 5) were obtained for each transition step in the proposed mechanisms shown in Figure 3:

$$\Delta H^\ddagger = E_a + RT \quad (3)$$

$$A = \frac{ek_B T}{h} e^{\frac{\Delta S^\ddagger}{R}} \quad (4)$$

$$\Delta G^\ddagger = \Delta H^\ddagger - T\Delta S^\ddagger \quad (5)$$

where k_B is Boltzmann's constant, T is the temperature at which the measurements were performed (in Kelvin), h is Planck's constant, and R is the gas constant. ΔS^\ddagger represents the difference between the entropy of each reactant or intermediate and its subsequent transition state; a negative value indicates that the system becomes more ordered at the transition state, and indicates the presence of an entropic barrier.

Equilibrium Experiments

Based on the kinetics experiments at various temperatures, the PPI \rightarrow PPII and PPII \rightarrow PPI transitions were assumed to have reached equilibrium 24 h and 150 h, respectively, after the initiation of the transition. The abundance of each conformer at equilibrium was calculated by integrating the CCS region using OriginPro 9.0.0 software. An equilibrium constant (K_{eq}) was calculated for each conformer at each temperature by ratioing its abundance to that of the initial conformer in the transition (conformer A for the PPI \rightarrow PPII transition, and conformer F for the PPII \rightarrow PPI transition). By fitting $\ln(K_{eq})$ versus $1/T$, the enthalpy (ΔH) and entropy (ΔS) changes were determined using the Van't Hoff equation (Equation 6),

$$\ln(K_{eq}) = \frac{-\Delta H}{R} \frac{1}{T} + \frac{\Delta S}{R} \quad (6)$$

$$\Delta G = \Delta H - T\Delta S \quad (7)$$

where T and R correspond to the temperature (in K) and the universal gas constant, respectively. The change in the Gibbs free energy (ΔG) can further be calculated using Equation 7. Equilibrium experiments were done in triplicate for each transition direction and at each of the nine temperatures: 15, 23, 30, 32.5, 35, 37.5, 40, 42.5, and 45°C. The solution was incubated in a water bath to maintain the desired temperature until the end of the experiment.

Molecular Modeling

Molecular dynamics (MD) simulations were performed on Pro13 [M + 2H]²⁺ ions on Linux workstations using Insight II 2005 (Accelrys Inc., San Diego, CA, USA). The MD methods have been described in detail in previous work [14, 15]; here, only a brief review is provided. Initial geometries of the [Pro13 + 2H]²⁺ ions with various distributions of *cis/trans* peptide bonds were

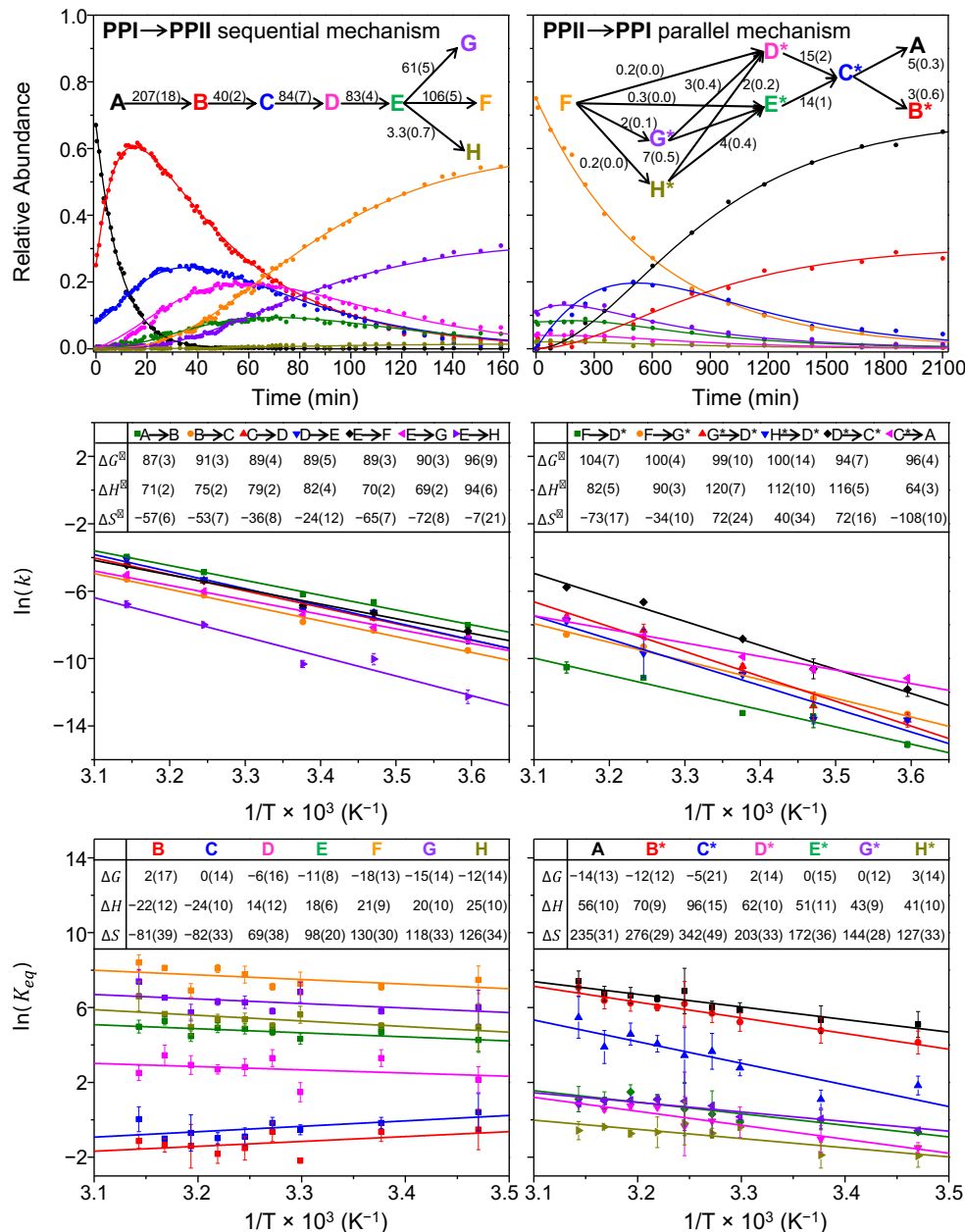


Figure 3. Kinetic and thermodynamic parameters for the PPI→PPII (left side) and PPII→PPI (right side) transitions. Top: relative abundance of different conformers as a function of transition time at 23°C. The best mechanism used to fit the data together with the obtained rate constant values are also shown. Middle: Arrhenius plots of the rate constants at 5, 15, 23, 35, and 45°C. The calculated Arrhenius activation parameters are used to derive transition state thermochemistry; only six transition steps for the PPII→PPI transition are shown here, and the other six steps are provided in Supporting Information (Supplementary Figure S33). Bottom: Van't Hoff plot of the equilibrium constants over a temperature range of 15–45°C. The number shown in parenthesis indicates standard deviation, and color coding for each conformer is the same as in Figure 2

generated. The locations of the protons were assumed to be at the N-terminus and the nitrogen atom of the sixth proline residue [14, 15]. The preparation for simulation was performed in the Discover_3 module equipped with the extensible systematic force field (ESFF). Then MD simulations were carried out at 300 K for a minimum of 0.25 ns (up to 2.0 ns) using ESFF and a dielectric constant of 1.0. For the obtained lowest-energy

conformations, the cross section values were calculated using the trajectory method in MOBCAL (Indiana University, Bloomington, IN, USA) [19] and were compared with the experimental values to determine the candidate Pro13 intermediate conformations in solution. The geometry chosen as the representative has calculated cross section within $\pm 2.0\%$ of the experimental value and the smallest difference from the experimental value. The

representative structure should also agree with the transition pathway determined from the experimental analysis.

Results and Discussion

Precursor PPI or PPII helices were created by incubation in either propanol or water, respectively. As the system evolves to equilibrium upon immersion in the new solvent, the ensemble of solution intermediates is monitored by measuring the ion mobility distributions of the dried $[\text{Pro13} + 2\text{H}]^{2+}$ species over time [12, 49]. As the same solution is sampled at each time point in this experiment, changes in the distribution of gas-phase conformers are due to changes in the originating solution population. Figure 2 shows examples of the distributions at different time points. Immediately after PPI is transferred to the aqueous environment, two peaks are observed: a large peak, at a cross section of $\Omega = 323 \text{ \AA}^2$; and, a smaller one, at $\Omega = 312 \text{ \AA}^2$. In contrast, upon immersing the aqueous PPII helix into propanol, the distribution is dominated by the sharp peak at $\Omega = 288 \text{ \AA}^2$. Comparisons of measured cross sections with calculated values for candidate geometries generated by molecular modeling simulations allow us to assign the $\Omega = 323 \text{ \AA}^2$ peak to the PPI helix (conformer A), and ions with $\Omega = 288 \text{ \AA}^2$ to the PPII helix (conformer F) [14]. Based on prior molecular dynamic (MD) simulations of PPI and PPII, the two protons were assumed to be located on the N-terminus and the nitrogen atom of the sixth residue [14, 15] (see below for detailed discussion). Over time, the precursors evolve into new structures. Within ~ 1 h, the PPI precursor all but vanishes; the PPII peak decays more slowly. The distributions for each solvent system are very different over time—an indication that the mechanism for PPI→PPII folding in water is not the same as that for PPII→PPI folding in 1-propanol. Eight structural types are resolved: peaks A and F, as well as six peaks corresponding to intermediates B through E, G, and H (see [Supporting Information](#)). At long times (>160 min after initiating the transition from PPI, and >2100 min for PPII), each system equilibrates, and no further changes are detectable.

We note that conformers with the same experimental CCS values were found for both the PPI→PPII and PPII→PPI transitions. Therefore, the solution-phase intermediate conformations proposed for the PPI→PPII transition according to prior MD simulations [10] are considered to represent the intermediate states observed for the reverse PPII→PPI transition. However, as we have not modeled all of the possible *cis/trans* combinations [14], we cannot rule out the possibility that different solution populations may generate dehydrated structures that have similar CCS values. Likewise, the initial protonation site on the nitrogen atom of the sixth residue may be mobile, and migration of the proton may also lead to different solution populations that have similar CCS values. As a result, we have designated the conformers in the PPII→PPI transition with an asterisk *.

Analysis of the data in Figure 2 provides insight into folding mechanisms. Figure 3 shows the integrated peak areas for the distributions shown in Figure 2, as well as data recorded for other times. Putative mechanisms are tested by fitting sets of differential rate equations to the experimental kinetics and assessing the agreement between fits for different assumed mechanisms and measurements. For PPI→PPII, the initial steps occur sequentially: $\text{PPI(A)} \rightarrow \text{B} \rightarrow \text{C} \rightarrow \dots$ (as shown in Figure 3). Among all the candidate transition pathways that we explored for the PPI→PPII transition, the transition mechanism selected in this study (Figure 3, top left) clearly shows the best fit to our experimental data [14]. Using the abundance profile obtained at 45°C , we compared the proposed transition route (Figure S8) with an additional 12 different fitting models that do not generate good fits for the experimental data (Figures S9 to S20). The residual sum of squares for each of the explored mechanisms is shown in Table S7.

Additional information about the transition mechanism of the PPI→PPII transition comes from molecular modeling studies [14]. Cross section calculations for model structures indicate that the first two intermediates (B and C) in the PPI→PPII transition arise from sequential *cis*→*trans* conversion from the N-terminus of the peptide [14]. The N-terminal backbone carbonyl groups, which are in close proximity to the protonated N-terminus of the ideal PPI structure, are accessible to water; thus, the PPI→PPII transition initiates from this side. Flipping of the first two peptide bonds yields intermediate B, and flipping of the third yields intermediate C [14]. Based on solvent accessibility, it might be expected that the PPI→PPII transformation proceeds to completion by sequentially unravelling additional adjacent residues from the N-terminal side. But, this is not the case. After flipping the first three bonds, a *cis*→*trans* rotation near the center of the peptide is observed [14].

For the PPII→PPI transition induced by dilution of PPII into 1-propanol, the kinetics cannot be accurately represented by a sequential mechanism. Instead, the mechanism that most closely represents the data (Figure 3, top right) involves a parallel process early in the transition; divergent pathways then converge to the common intermediate, C*, to produce the final PPI helix. A number of candidate transition pathways have very similar fittings (Figures S21 to S26) to our proposed mechanism for the PPII→PPI transition (Figure 3, top right). However, all of these transition mechanisms involve a partially parallel transition pathway. Using the residual sum of squares, we investigated six candidate models that generate good fits for the experimental data points (Figures S21 to S26) and six transition routes (Figures S27 to S32) that do not. Values for the residual sum of squares for each of these fitting models are tabulated in Table S8, and the proposed mechanism has the smallest sum of the residual sum of squares.

The complexity of how these transformations occur begs the question: Why do they occur? To address this, we investigated the thermodynamics of folding. Insight about transition state barriers is obtained from temperature-dependent kinetics studies, from 5 to 45°C (see [Supporting Information](#)). Arrhenius

plots (Figure 3) yield pre-exponential factors and activation energies that can be converted into transition state free energies (ΔG^\ddagger), enthalpies (ΔH^\ddagger), and entropies (ΔS^\ddagger) (see [Experimental](#), and Tables S2, S3).

The exceptional dynamic range of mass spectrometry-based techniques allows us to monitor equilibria and generate Van't Hoff plots (Figure 3), even for species that differ in abundance by factors of $>10^5$. From these, we determine ΔG , ΔH , and ΔS for each intermediate relative to the initial state.

As is seen in the left panel of Figure 2 and Figure S34, the CCS of conformer A observed in the equilibrium distribution (318 \AA^2) of the PPI \rightarrow PPII transition is slightly smaller than the one found in the initial distribution (322 \AA^2). A shoulder corresponding to this more compact gas-phase conformer is also present on the peak of conformer A in the initial stages of

the transition (Figure 2). Using MD simulations, we were unable to identify a likely solution conformation that would generate this gas-phase conformer, designated A'. As our equilibrium calculations involve A', not A, this may cause some deviations in the absolute values of ΔH , ΔS , and ΔG for the intermediate states in the PPI \rightarrow PPII transition. However, the trends observed with ΔH and ΔS should not be affected by the presence of a different starting geometry.

The sequential PPI \rightarrow PPII and parallel PPII \rightarrow PPI pathways determined from the kinetics analyses are combined with the thermodynamic evaluations to create the energy landscapes shown in Figure 4. The sequential PPI \rightarrow PPII hydration transition is exoergic ($\Delta G_{\text{PPI} \rightarrow \text{PPII}} = -18 \pm 13 \text{ kJ} \cdot \text{mol}^{-1}$), with similar transition state barriers ranging from $\Delta G_{\text{A} \rightarrow \text{B}}^\ddagger = 87 \pm 3$ to $\Delta G_{\text{E} \rightarrow \text{H}}^\ddagger = 96 \pm 9 \text{ kJ} \cdot \text{mol}^{-1}$ (Table S3) for individual steps.

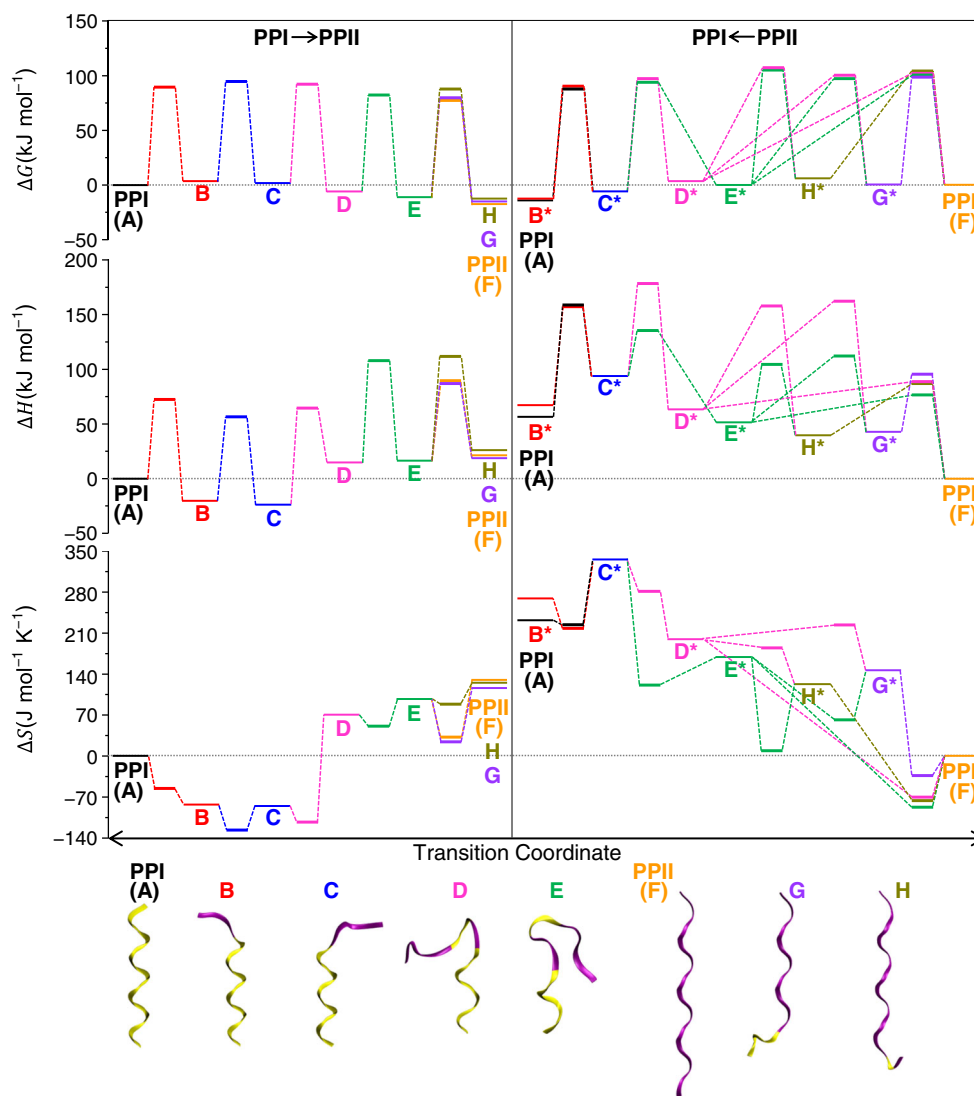


Figure 4. Experimental energy diagrams showing ΔG , ΔH , and ΔS for proposed pathways and intermediates (top: change in Gibbs free energy; middle: change in enthalpy; bottom: change in entropy) shown as a function of transition coordinate for the PPI \rightarrow PPII transition (left) and the PPII \rightarrow PPI transition (right, read from right to left). Color coding for each conformer is the same as in Figure 2, and the asterisk * indicates the uncertainty in the conformer assignments. Lower panel: structures for PPI, PPII, and proposed structures for intermediates found in the PPI \rightarrow PPII transitions, as determined through MD simulations [14]. The *cis* residues are shown as yellow ribbons, and the *trans* residues are shown as purple ribbons

The enthalpy and entropy diagrams provide a more detailed understanding of why the PPI→PPII transition occurs. From the ΔH plot, we learn that while the overall process is endothermic, the first step is exothermic ($\Delta H_{A\rightarrow B} = -22 \pm 12 \text{ kJ}\cdot\text{mol}^{-1}$), proceeding over a barrier of $\Delta H_{A\rightarrow B}^\ddagger = 71 \pm 2 \text{ kJ}\cdot\text{mol}^{-1}$. Interaction of exposed carbonyl groups in intermediate B with water molecules is energetically favorable; however, this imposes an entropic penalty of $\Delta S_{A\rightarrow B}^\ddagger = -57 \pm 6 \text{ J}\cdot\text{mol}^{-1}\cdot\text{K}^{-1}$ at the transition state and $\Delta S_{A\rightarrow B} = -81 \pm 39 \text{ J}\cdot\text{mol}^{-1}\cdot\text{K}^{-1}$ for formation of the B intermediate. That is, in order to form the more stable intermediate B, the system must become more ordered. The same is true for the B→C transition.

The endothermicity of the next step ($\Delta H_{C\rightarrow D} = 38 \pm 16 \text{ kJ}\cdot\text{mol}^{-1}$) is surprising and is key to understanding the mechanism. Why would the system choose a *cis*→*trans* rotation near the center of the peptide instead of flipping the next adjacent *cis*→*trans* peptide bond? ΔS is the clue! It appears that the order that is imposed upon *cis*→*trans* conversion of the next adjacent, (fourth) peptide bond is beyond what can be accommodated energetically (i.e., ΔH). Therefore, the system abandons this mechanism and instead rotates near the peptide center. Such a motion sweeps through a substantial volume of the surrounding solvent, inducing a large loss of order ($\Delta S_{C\rightarrow D} = 151 \pm 50 \text{ J}\cdot\text{mol}^{-1}\cdot\text{K}^{-1}$) and providing the impetus ($-T_{298}\Delta S_{C\rightarrow D} = -45 \pm 14 \text{ kJ}\cdot\text{mol}^{-1}$) to continue folding. Examination of late steps shows that they are thermoneutral (e.g., $\Delta H_{D\rightarrow E} = 4 \pm 13 \text{ kJ}\cdot\text{mol}^{-1}$, see Table S5 for other values). Concurrently, the overall entropy increases slightly ($\Delta S_{D\rightarrow PPII} = 61 \pm 48 \text{ J}\cdot\text{mol}^{-1}\cdot\text{K}^{-1}$) as intermediate D folds to the final PPII helix.

These data also explain why the PPII→PPI transition utilizes a parallel multi-pathway mechanism. This transformation is highly endothermic, $\Delta H_{PPII\rightarrow PPI} = 56 \pm 10 \text{ kJ}\cdot\text{mol}^{-1}$. No early steps are favorable. The PPII(F) precursor encounters large barriers ($\Delta G_{F\rightarrow D}^\ddagger = 104 \pm 7 \text{ kJ}\cdot\text{mol}^{-1}$, $\Delta G_{F\rightarrow E}^\ddagger = 103 \pm 4 \text{ kJ}\cdot\text{mol}^{-1}$, $\Delta G_{F\rightarrow G}^\ddagger = 100 \pm 4 \text{ kJ}\cdot\text{mol}^{-1}$, $\Delta G_{F\rightarrow H}^\ddagger = 106 \pm 8 \text{ kJ}\cdot\text{mol}^{-1}$) regardless of the choice of path. Dehydration of PPII in 1-propanol destabilizes all of the early intermediates and transition states, such that all initial steps are endothermic. With no good option, the PPII population splits along multiple high-energy routes using an increase in system entropy to find the late intermediate C*. That is, key to forming PPI helix is a large-scale search for intermediate C*. The decreased population of intermediates between F and C* indicate that these steps, although slower, occur more cooperatively than in the reverse step-by-step PPI→PPII transition. That local environment leads to such mechanistic disparity illustrates the importance of experimental measurements in characterizing folding landscapes.

Conclusions

The remarkable solution dependence of the PPI and PPII helices of polyproline has attracted considerable attention for more than 50 years. Although early studies suggested the

presence of *cis/trans* isomers for such oligomers, few options for characterizing such species or following how these systems evolve from one form into another existed. The IM-MS studies presented here allow us to follow folding pathways in remarkable detail, and the thermodynamic measurements for specific transition states and intermediates provide new insight into underlying mechanisms of peptide folding. Early PPI→PPII intermediates are energetically favorable because of hydration of the peptide backbone. Late intermediates are enthalpically unfavorable; however, key peptide bonds continue flipping because of a stepwise increase in system entropy upon formation of each successive structure. The reverse PPII→PPI transition, induced when hydrated-PPII is immersed in 1-propanol, proceeds by an entirely different mechanism. Although the free energy change for individual steps as well as the overall change for the reverse PPII→PPI process is similar to values determined for the forward PPI→PPII transition, we see immediately that the underlying thermodynamic factors that drive the reaction are different. Essentially, all of the intermediates and transition states are destabilized as the system folds in reverse as propanol replaces water. With no energetically favorable first steps, the PPII→PPI dehydration transition becomes entropically driven. In recent years, these transitions have been investigated theoretically [50–53]. It will be interesting to see if theoretical calculations can capture the fundamental essence of the folding differences of these systems in different solvents.

Acknowledgments

The authors thank David Smiley and the DiMarchi Laboratory at Indiana University for help with the peptide synthesis. The instrumentation used in these studies was developed in part from a grant from the NIH (RC1GM090797-02) and through support from the Waters Corporation.

References

1. Anfinsen, C.B., Haber, E., Sela, M., White Jr., F.H.: The kinetics of formation of native ribonuclease during oxidation of the reduced polypeptide chain. *Proc. Natl. Acad. Sci. U. S. A.* **47**, 1309–1314 (1961)
2. Dill, K.A., MacCallum, J.L.: The protein-folding problem, 50 Years on. *Science* **338**, 1042–1046 (2012)
3. Kim, P.S., Baldwin, R.L.: Intermediates in the folding reactions of small proteins. *Annu. Rev. Biochem.* **59**, 631–660 (1990)
4. Matthews, C.R.: Pathways of protein folding. *Annu. Rev. Biochem.* **62**, 653–683 (1993)
5. Bryngelson, J.D., Wolynes, P.G.: Spin glasses and the statistical mechanics of protein folding. *Proc. Natl. Acad. Sci. U. S. A.* **84**, 7524–7528 (1987)
6. Dill, K.A., Chan, H.S.: From Levinthal to pathways to funnels. *Nat. Struct. Biol.* **4**, 10–19 (1997)
7. Englander, S.W., Mayne, L.: The nature of protein folding pathways. *Proc. Natl. Acad. Sci. U. S. A.* **111**, 15873–15880 (2014)
8. Shea, J.-E., Brooks III, C.L.: From folding theories to folding proteins: a review and assessment of simulation studies of protein folding and unfolding. *Annu. Rev. Phys. Chem.* **52**, 499–535 (2001)
9. Fersht, A.R.: From the first protein structures to our current knowledge of protein folding: delights and skepticisms. *Nat. Rev. Mol. Cell Biol.* **9**, 650–654 (2008)
10. Hoaglund-Hyzer, C.S., Counterman, A.E., Clemmer, D.E.: Anhydrous protein ions. *Chem. Rev.* **99**, 3037–3079 (1999)

11. Bohrer, B.C., Merenbloom, S.I., Koeniger, S.L., Hilderbrand, A.E., Clemmer, D.E.: Biomolecule analysis by ion mobility spectrometry. *Annu. Rev. Anal. Chem.* **1**, 293–327 (2008)
12. Wyttenbach, T., Pierson, N.A., Clemmer, D.E., Bowers, M.T.: Ion mobility analysis of molecular dynamics. *Annu. Rev. Phys. Chem.* **65**, 175–196 (2014)
13. Shi, L., Holliday, A.E., Khanal, N., Russell, D.H., Clemmer, D.E.: Configurationally-coupled protonation of polyproline-7. *J. Am. Chem. Soc.* **137**, 8680–8683 (2015)
14. Shi, L., Holliday, A.E., Shi, H., Zhu, F., Ewing, M.A., Russell, D.H., Clemmer, D.E.: Characterizing intermediates along the transition from polyproline I to polyproline II using ion mobility spectrometry-mass spectrometry. *J. Am. Chem. Soc.* **136**, 12702–12711 (2014)
15. Counterman, A.E., Clemmer, D.E.: Anhydrous polyproline helices and globules. *J. Phys. Chem. B* **108**, 4885–4898 (2004)
16. Counterman, A.E., Clemmer, D.E.: *Cis-trans* signatures of proline-containing tryptic peptides in the gas phase. *Anal. Chem.* **74**, 1946–1951 (2002)
17. Pierson, N.A., Chen, L., Russell, D.H., Clemmer, D.E.: *Cis-trans* isomerizations of proline residues are key to bradykinin conformations. *J. Am. Chem. Soc.* **135**, 3186–3192 (2013)
18. Warnke, S., Baldauf, C., Bowers, M.T., Pagel, K., von Helden, G.: Photodissociation of conformer-selected ubiquitin ions reveals site-specific *cis/trans* isomerization of proline peptide bonds. *J. Am. Chem. Soc.* **136**, 10308–10314 (2014)
19. Mesleh, M.F., Hunter, J.M., Shvartsburg, A.A., Schatz, G.C., Jarrold, M.F.: Structural information from ion mobility measurements: effects of the long-range potential. *J. Phys. Chem.* **100**, 16082–16086 (1996)
20. Ruotolo, B.T., Giles, K., Campuzano, I., Sandercock, A.M., Bateman, R.H., Robinson, C.V.: Evidence for macromolecular protein rings in the absence of bulk water. *Science* **310**, 1658–1661 (2005)
21. Ruotolo, B.T., Robinson, C.V.: Aspects of native proteins are retained in vacuum. *Curr. Opin. Chem. Biol.* **10**, 402–408 (2006)
22. Silveira, J.A., Fort, K.L., Kim, D., Servage, K.A., Pierson, N.A., Clemmer, D.E., Russell, D.H.: From solution to the gas phase: stepwise dehydration and kinetic trapping of substance p reveals the origin of peptide conformations. *J. Am. Chem. Soc.* **135**, 19147–19153 (2013)
23. Chen, L., Chen, S.-H., Russell, D.H.: An experimental study of the solvent-dependent self-assembly/disassembly and conformer preferences of gramicidin A. *Anal. Chem.* **85**, 7826–7833 (2013)
24. Bleiholder, C., Dupuis, N.F., Wyttenbach, T., Bowers, M.T.: Ion mobility-mass spectrometry reveals a conformational conversion from random assembly to B-sheet in amyloid fibril formation. *Nat. Chem.* **3**, 172–177 (2011)
25. Fenn, J.B., Mann, M., Meng, C.K., Wong, S.F., Whitehouse, C.M.: Electrospray ionization for mass spectrometry of large biomolecules. *Science* **246**, 64–71 (1989)
26. Steinberg, I.Z., Harrington, W.F., Berger, A., Sela, M., Katchalski, E.: The configurational change of poly-L-proline in solution. *J. Am. Chem. Soc.* **82**, 5263–5279 (1960)
27. Forsythe, K.H., Hopfinger, A.J.: The influence of solvent on the secondary structures of poly(L-alanine) and poly(L-proline). *Macromolecules* **6**, 423–437 (1973)
28. Kuemin, M., Engel, J., Wennemers, H.: Temperature-induced transition between polyproline I and II helices: quantitative fitting of hysteresis effects. *J. Pept. Sci.* **16**, 596–600 (2010)
29. Schimmel, P.R., Flory, P.J.: Conformational energy and configurational statistics of poly-L-proline. *Proc. Natl. Acad. Sci. U. S. A.* **58**, 52–59 (1967)
30. Traub, W., Shmueli, U.: Structure of poly-L-proline I. *Nature* **198**, 1165–1166 (1963)
31. Adzhubei, A.A., Sternberg, M.J., Makarov, A.A.: Polyproline-II helix in proteins: structure and function. *J. Mol. Biol.* **425**, 2100–2132 (2013)
32. Rath, A., Davidson, A.R., Deber, C.M.: The structure of “unstructured” regions in peptides and proteins: role of the polyproline II helix in protein folding and recognition. *Biopolymers (Peptide Sci)* **80**, 179–185 (2005)
33. Shi, Z., Chen, K., Liu, Z., Kallenbach, N.R.: Conformation of the backbone in unfolded proteins. *Chem. Rev.* **106**, 1877–1897 (2006)
34. Schweitzer-Stenner, R.: Conformational propensities and residual structures in unfolded peptides and proteins. *Mol. BioSyst.* **8**, 122–133 (2012)
35. IUPAC-IUB Commission on Biochemical Nomenclature: Abbreviations and symbols for the description of the conformation of polypeptide chains. Tentative rules (1969). *Biochemistry* **9**, 3471–3479 (1970)
36. Chandrudu, S., Simerska, P., Toth, I.: Chemical methods for peptide and protein production. *Molecules* **18**, 4373–4388 (2013)
37. Mason, E.A., McDaniel, E.W.: Transport properties of ions in gases. Wiley, New York (1988)
38. Revercomb, H.E., Mason, E.A.: Theory of plasma chromatography/gaseous electrophoresis. *Anal. Chem.* **47**, 970–983 (1975)
39. Shvartsburg, A.A., Jarrold, M.F.: An exact hard-spheres scattering model for the mobilities of polyatomic ions. *Chem. Phys. Lett.* **261**, 86–91 (1996)
40. Wyttenbach, T., von Helden, G., Batka, J.J., Carlat, D., Bowers, M.T.: Effect of the long-range potential on ion mobility measurements. *J. Am. Soc. Mass Spectrom.* **8**, 275–282 (1997)
41. McLean, J.A., Ruotolo, B.T., Gillig, K.J., Russell, D.H.: Ion mobility-mass spectrometry: a new paradigm for proteomics. *Int. J. Mass Spectrom.* **240**, 301–315 (2005)
42. Tang, K., Shvartsburg, A.A., Lee, H.-N., Prior, D.C., Buschbach, M.A., Li, F., Tolmachev, A.V., Anderson, G.A., Smith, R.D.: High-sensitivity ion mobility spectrometry/mass spectrometry using electrodynamic ion funnel interfaces. *Anal. Chem.* **77**, 3330–3339 (2005)
43. Kanu, A.B., Dwivedi, P., Tam, M., Matz, L., Hill Jr., H.H.: Ion mobility-mass spectrometry. *J. Mass Spectrom.* **43**, 1–22 (2008)
44. Shaffer, S.A., Tang, K.Q., Anderson, G.A., Prior, D.C., Udseth, H.R., Smith, R.D.: A novel ion funnel for focusing ions at elevated pressure using electrospray ionization mass spectrometry. *Rapid Commun. Mass Spectrom.* **11**, 1813–1817 (1997)
45. Hoaglund, C.S., Valentine, S.J., Sporleder, C.R., Reilly, J.P., Clemmer, D.E.: Three-dimensional ion mobility/TOFMS analysis of electrosprayed biomolecules. *Anal. Chem.* **70**, 2236–2242 (1998)
46. Bleiholder, C., Do, T.D., Wu, C., Economou, N.J., Bernstein, S.S., Buratto, S.K., Shea, J.-E., Bowers, M.T.: Ion mobility spectrometry reveals the mechanism of amyloid formation of A β (25–35) and its modulation by inhibitors at the molecular level: epigallocatechin gallate and scyllo-inositol. *J. Am. Chem. Soc.* **135**, 16926–16937 (2013)
47. Loo, J.A., Edmonds, C.G., Smith, R.D.: Primary sequence information from intact proteins by electrospray ionization tandem mass spectrometry. *Science* **248**, 201–204 (1990)
48. Merenbloom, S.I., Flick, T.G., Williams, E.R.: How hot are your ions in T-wave ion mobility spectrometry? *J. Am. Soc. Mass Spectrom.* **23**, 553–562 (2012)
49. Clemmer, D.E., Jarrold, M.F.: Ion mobility measurements and their applications to clusters and biomolecules. *J. Mass Spectrom.* **32**, 577–592 (1997)
50. Moradi, M., Babin, V., Roland, C., Sagui, C.: A classical molecular dynamics investigation of the free energy and structure of short polyproline conformers. *J. Chem. Phys.* **133**, 125104–125122 (2010)
51. Moradi, M., Babin, V., Roland, C., Darden, T.A., Sagui, C.: Conformations and free energy landscapes of polyproline peptides. *Proc. Natl. Acad. Sci. U. S. A.* **106**, 20746–20751 (2009)
52. Moradi, M., Lee, J.G., Babin, V., Roland, C., Sagui, C.: An ab initio and classical molecular dynamics investigation. *Int. J. Quantum Chem.* **110**, 2865–2879 (2010)
53. Chiang, Y., Lin, Y., Homg, J.: Stereoelectronic effects on the transition barrier of polyproline conformational interconversion. *Protein Sci.* **18**, 1967–1977 (2009)